IOP Publishing Bioinspiration & Biomimetics
Bioinspir. Biomim. 9 (2014) 036008 (8pp) doi:10.1088/1748-3182/9/3/036008

Flexible propulsors in ground effect

Daniel B Quinn[1], **George V Lauder**[2] **and Alexander J Smits**[1,3]

[1] Department of Mechanical and Aerospace Engineering, Princeton University, Princeton, NJ 08544, USA
[2] Department of Organismal and Evolutionary Biology, Harvard University, Cambridge, MA 02138, USA
[3] Monash University, Victoria, Australia

E-mail: danielq@princeton.edu

Received 17 October 2013, revised 28 February 2014
Accepted for publication 4 March 2014
Published 26 March 2014

Abstract

We present experimental evidence for the hydrodynamic benefits of swimming 'in ground effect', that is, near a solid boundary. This situation is common to fish that swim near the substrate, especially those that are dorsoventrally compressed, such as batoids and flatfishes. To investigate flexible propulsors in ground effect, we conduct force measurements and particle image velocimetry on flexible rectangular panels actuated at their leading edge near the wall of a water channel. For a given actuation mode, the panels swim faster near the channel wall while maintaining the same propulsive economy. In conditions producing net thrust, panels produce more thrust near the ground. When operating in resonance, swimming near the ground can also increase propulsive efficiency. Finally, the ground can act to suppress three-dimensional modes, thereby increasing thrust and propulsive efficiency. The planform considered here is non-biological, but the hydrodynamic benefits are likely to apply to more complex geometries, especially those where broad flexible propulsors are involved such as fish bodies and fins. Such fish could produce more thrust by swimming near the ground, and in some cases do so more efficiently.

Keywords: fluid dynamics, ground effect, fluid-structure interaction, biolocomotion, benthic fish

(Some figures may appear in colour only in the online journal)

1. Introduction

Swimming near a solid boundary can lead to significant hydrodynamic benefits. Steelhead trout, for example, can reduce their cost of transport by swimming near the walls of a channel [1], and buoyant mandarin fish use less power when hovering near the substrate [2]. Some benthic fish use the substrate via direct contact, also known as fin 'walking' [3] or 'punting' [4], but here we focus on the effects of propulsors close to, but not touching, solid boundaries. Even without making contact, near-boundary swimmers experience different hydrodynamics, and in many cases adjust their body kinematics accordingly [5–8].

The properties of static lifting surfaces moving parallel to a solid boundary, or 'steady ground effect', has been widely studied (see, for example, the review by Rozhdestvensky [9]). In the steady case, fins/wings produce more lift near the ground due to a combination of (a) decelerated flow beneath the lifting surface resulting in higher underside pressures, and (b) a reduction in wing-tip vortices resulting in less induced drag. The benefits of steady ground effect have led to a broad literature describing the advantages of birds [10–13] and fish [14, 15] gliding near solid boundaries. Since these effects scale with the distance to the boundary normalized by the chord, they are most relevant for laterally compressed species gliding near a side wall or dorsoventrally compressed species gliding near the substrate/ground.

In contrast, much less is known about 'unsteady ground effect', where fins or wings are oscillating and undulating to produce thrust near a solid boundary. Such near-ground propulsion is interesting from both a biological and engineering standpoint, because it is reasonable to suspect that the increase in lift in the steady case translates to an increase in thrust in the unsteady case. This was predicted theoretically [16, 17] and has been demonstrated experimentally for the simple case of a pitching rigid airfoil in water [18]. Ground

Table 1. Panel specifications. Stiffness is quantified by the flexural rigidity $EI = Es\delta^3/(12(1-\nu^2))$, with elastic modulus E, panel span s, panel thickness δ, and Poisson's ratio ν.

Panel	E (GPa)	δ (mm)	EI (N m^2)
A	1.7	0.77	1.1×10^{-2}
B	1.8	0.32	8.1×10^{-4}
C	3.8	0.11	6.9×10^{-5}

effect has also been shown to increase the unsteady forces on flapping beetle-like synthetic wings during take-off [19]. A separate study, however, considered the swimming speeds of a stingray-inspired flexible fin and found no significant benefits of near-ground swimming [20].

As unsteady ground effect is a relatively new area of study, it remains unclear exactly when near-ground benefits apply to unsteady propulsion. The goal of the current study is to explore this parameter space, as well as to answer some additional questions: how much do near-ground thrust benefits increase the swimming speed, what role does flexibility play near the ground, where in the oscillation cycle do the hydrodynamic benefits occur, and can a propulsor produce thrust more efficiently near the ground? No previous studies, for example, reported a significant change in the measured propulsive efficiency of the unsteady motion. A major finding of the present work is that the propulsive efficiency of oscillating propulsors can increase in ground effect under certain conditions. The goal of the study was not to create a biomimetic fin, but rather to mimic the close proximity to the substrate of a broad-bodied flexible propulsor. Thus, in order to isolate the effects of flexibility and ground proximity, an oscillating flexible rectangular panel was used as a model undulating fin. A simple robotic model was chosen in place of live fish to offer precise control of fin amplitude, oscillation frequency, and ground proximity.

2. Experimental methods

2.1. Panel actuation

The leading edge of rectangular polyethylene panels was actuated with sinusoidal heaving oscillations, sending a propulsive traveling wave along the body. Three panels of varying flexibility were tested, with panel 'A' being the stiffest and panel 'C' the most flexible (see table 1). Each panel had a chord length $c = 195$ mm and a span $s = 150$ mm. The panels were immersed in a recirculating water channel and actuated from above the surface. Further details of the actuation mechanism are given by Lauder *et al* [21, 22]. The heaving amplitude a was set to 20 mm ($a/c = 0.1$) for all trials (see figure 1), while the heaving frequency f ranged from 0 to 3.5 Hz in intervals of 0.125 Hz. In self-propelled swimming trials, the free stream velocity u_∞ ranged from 140 to 170 mm s^{-1}; in all other trials $u_\infty = 110$ mm s^{-1}. These parameters give a Reynolds number based on the chord (cu_∞/ν) ranging from 21 000 to 33 000 and a Strouhal number (fa'/u_∞; a' = trailing edge peak-to-peak amplitude) ranging from 0 to 0.9. The amplitude and frequency range were chosen

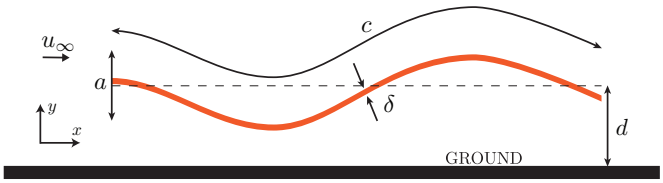

Figure 1. Length-scale definitions. The parameters shown are the chord length c, thickness δ, peak-to-peak heaving amplitude a, wall proximity d, and free stream velocity u_∞. The span s is into the page. The 'ground' is formed by the channel wall.

to include those observed in previous experiments on live freshwater stingrays [23].

The ground proximity d is defined as the average distance between the leading edge and the wall of the water channel (see figure 1). The minimum distance was $d = 40$ mm ($d/a = 2$), while the maximum was 140 mm ($d/a = 7$), at which point the panel was equidistant from the two sides of the channel. This condition will be referred to as $d/a \gg 1$. Due to the flexibility of the panel, the trailing edge passed as close as 15 mm from the wall, and therefore at the lower values of d the panel is expected to be within the boundary layer that is present on the wall of the channel. Note that free-swimming fish experience no such boundary layer as they swim along the substrate in quiescent water. While this is likely to affect the forces to some degree, the effect is presumed to be small. For a more thorough discussion see Quinn *et al* [18], where a potential flow solver was used to help identify the role of the viscous boundary layer in ground effect for rigid panels.

2.2. Force measurement

A force sensor (ATI Inc., Nano-17 SI-50-0.5) was mounted along the leading edge spar to measure hydrodynamic loads on the propulsor. In what follows, the net streamwise force ($\mathcal{F}_x$) will be referred to as the net thrust. For the heaving motion considered, the power input to the fluid ($\mathcal{P}$) is given by the lateral force ($\mathcal{F}_y$) multiplied by the (negative) lateral velocity of the leading edge ($-\dot{y}_{\mathrm{LE}}$). The instantaneous net thrust and power signals were filtered digitally (12 Hz low-pass 2nd-order Butterworth) and phase-averaged over a 10 s window. Time-averages were taken by averaging over this same set of cycles. Phase averages will be noted with a tilde (e.g. $\tilde{\mathcal{F}}_x$) and time averages with an overbar (e.g. $\bar{\mathcal{P}}$). To measure the self-propelled swimming speed (u_{SPS}), the flow speed of the water channel was adjusted manually until the magnitude of the time-averaged net thrust ($\bar{\mathcal{F}}_x$) was less than 2 mN. This threshold was chosen to be less than 5% of typical peak values in $\mathcal{F}_x$. All reported errors are based on the standard deviation of seven trials and the resolution of the force sensor.

2.3. Panel kinematics and flow visualization

To analyze the panel kinematics and surrounding flow field, 1024 × 1024 pixel images were taken at 200 Hz from beneath the water channel (Photron, FASTCAM 1024 PCI). The images were used to conduct particle image velocimetry (PIV) and to track the panel kinematics using an in-house edge tracking code. The laser sheet for PIV was in the x–y plane (see

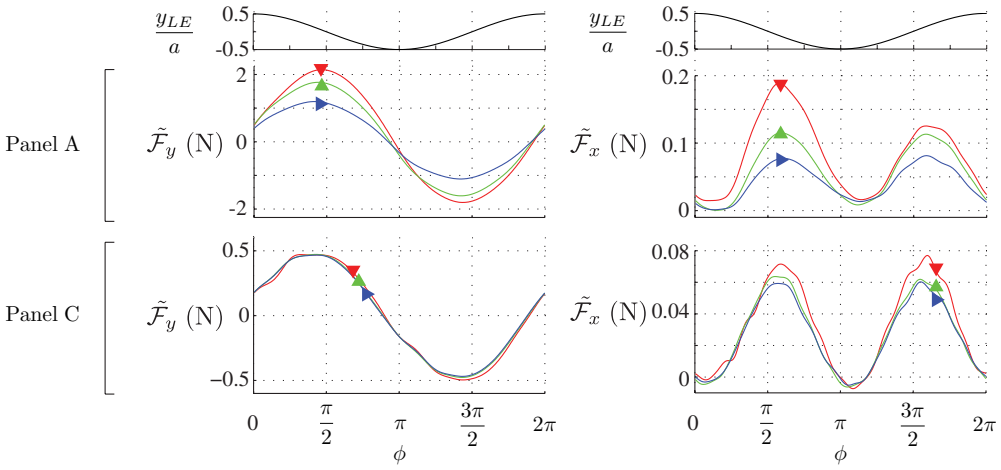

Figure 2. Phase-averaged lateral forces ($\tilde{\mathcal{F}}_y$) and net thrust ($\tilde{\mathcal{F}}_x$). $u_\infty = 110$ mm s^{-1}; $f = 2$ Hz. Ground proximities: $d/a = 2$, ▼; $d/a = 3$, ▲; $d/a \gg 1$, ►. Top row shows position of the leading edge as a reference. Error bars are omitted for cleanliness, but estimated to be $\pm$ 0.01 N for the data shown here.

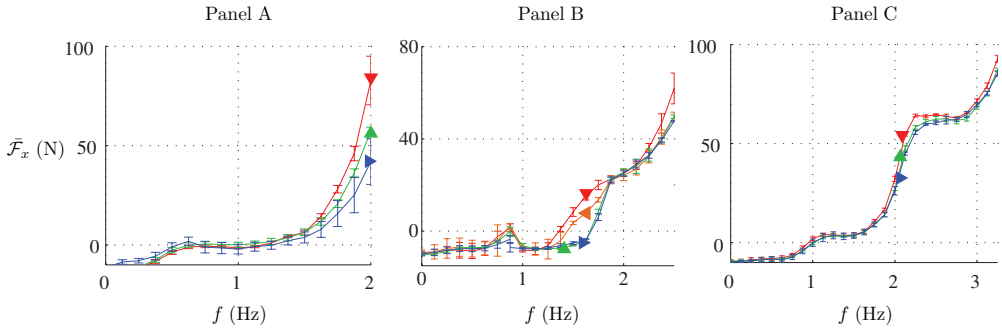

Figure 3. Time-averaged net thrust ($\bar{\mathcal{F}}_x$). Ground proximities: $d/a = 2.5$, ◄; other symbols as in figure 2. Error bars show +/− one standard error.

figure 1) at the midspan and was generated by a continuous 10W argon-ion laser (Coherent, Innova 70-C). The seeding particles were hollow silver-coated glass beads with an average diameter of 12 μm. The velocity field was calculated using Davis 8.1.3, the spatial cross-correlation algorithm developed by LaVision Inc. [24]. Nine passes with 50% overlap were conducted on the data: three with 128 × 128 pixel windows, three with 64 × 64, and three with 32 × 32.

3. Results

3.1. Force production

Figure 2 shows phase-averaged lateral forces ($\tilde{\mathcal{F}}_y$) and net thrust ($\tilde{\mathcal{F}}_x$) through the flapping cycle for the least (A) and most (C) flexible panels. The phase ϕ is defined with $\phi = 0$ corresponding to the moment the leading edge is farthest from the wall. As one might expect from a geometrical argument, $|\tilde{\mathcal{F}}_y|/|\tilde{\mathcal{F}}_x| = O(c/a)$ for both panels. In addition, the higher flexural rigidity of panel A leads to higher lateral forces. Two peaks per flapping cycle occur in the lateral force and the net thrust - one just after the panel is at mid downstroke, and one half a cycle later. For panel A, we see a significant increase due to ground effect in the magnitude of the lateral force and the thrust. At the closest ground proximity, the thrust is amplified most during the downstroke. A similar, but considerably smaller effect is seen for panel C.

To investigate bulk swimming performance, the time-averaged streamwise forces are shown in figure 3 over a range of frequencies. The appearance of plateaus in thrust was noted previously for this panel when operating far away from the ground, and it was attributed to chordwise resonance [25]. A panel is said to be ‘in resonance’ when its trailing amplitude passes through local maxima in frequency space. The more flexible panels pass through multiple resonant modes, and therefore multiple plateaus appear in the net thrust behavior. Resonance occurs just before each plateau and leads to increased thrust. Panel C, for example, experiences resonance when flapping at just over 1 Hz and again when flapping at just over 2Hz.

Figure 3 shows that net thrust increases near the ground in specific subsets of the frequency space considered. The first subset corresponds to high flapping frequencies for the more rigid panels. Panel A, for example, produces almost double the thrust at $d/a = 2$ when operating at its highest frequency. The second subset corresponds to the frequency range where panel C is operating in resonance and the time-averaged thrust increases near the ground. This effect relies on the flexibility of the propulsor. On either side of the frequency band where resonance occurs, panel C experiences no near-ground benefits. To capitalize on ground effect in

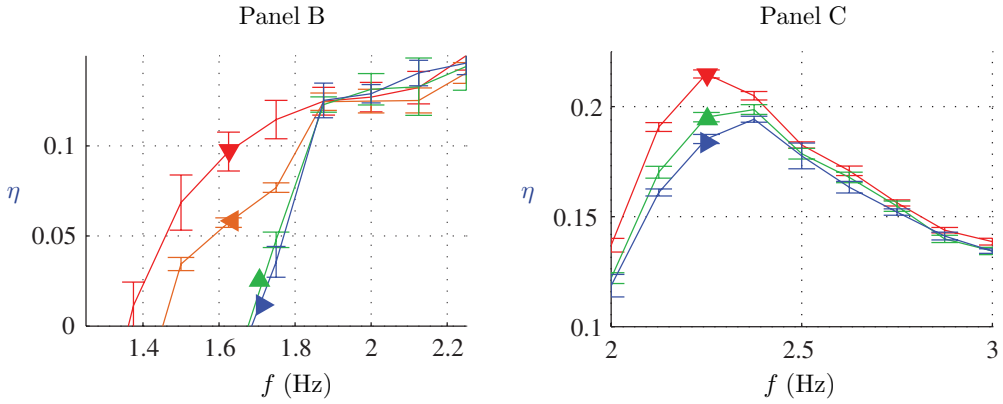

Figure 4. Propulsive efficiency ($\eta \equiv \bar{\mathcal{F}}_x u_\infty / \bar{\mathcal{P}}$). Left: panel B showing torsional mode suppression. Right: panel C operating near resonance. Symbols and error bars as in figure 3.

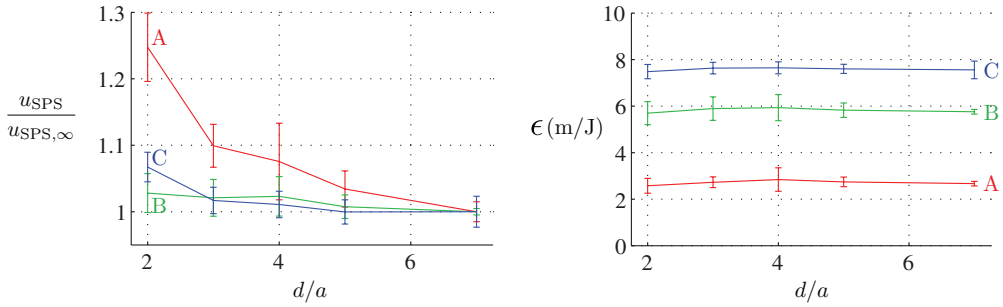

Figure 5. Self-propelled swimming near the ground. $f = 2$ Hz. Left: self-propelled swimming speed (u_{SPS}) compared to $d/a \gg 1$ value ($u_{\mathrm{SPS},\infty}$). Right: propulsive economy ($\Omega \equiv u_{\mathrm{SPS}}/\bar{\mathcal{P}}$). Panels indicated by letter. Error bars show +/− one standard error.

this frequency regime, panel C must operate at a resonant frequency.

The third subset of frequencies where thrust increases is the most unfamiliar of the three, because unlike the other two the effect involves three-dimensional kinematics. Between 1 and 2 Hz, panel B experiences excitation of its first spanwise mode. The superposition of chordwise and spanwise modes causes the trailing edge to twist about the x-axis. The transition to this torsional mode is marked by a sharp increase in the variance of the observed kinematics, but is quantified best by the sudden drop in time-averaged thrust occurring at 1 Hz. As the frequency increases past the resonant frequency of this spanwise mode, the time-averaged thrust rises rapidly as the spanwise mode is suppressed. The reason this effect is significant here is that the ground assists in inhibiting the three-dimensional mode. Thus, when $d/a = 2.5$ and $d/a = 2$, the frequency band over which the torsion occurs is narrower, and the thrust increase occurs at lower frequencies. When f =1.625 Hz, for example, panel B experiences net drag far from the ground, but net thrust near the ground, despite having the same actuation.

One way to quantitatively separate these three types of thrust increase is by considering the propulsive efficiency, $\eta \equiv \bar{\mathcal{F}}_x u_\infty / \bar{\mathcal{P}}$, a measure of the usefulness of the energy transmitted to the wake. The first type of thrust increase was not associated with an increase in efficiency. Thus, to within the experimental uncertainty, the propulsive efficiency of panel A was not affected by ground proximity. While it produced more thrust near the ground, it also required more power, and the net result was constant efficiency. The other forms of thrust increase, however, lead to increased efficiencies (see figure 4). Panels B and C (the two most flexible panels) both show increased efficiency near the ground: panel B when the three-dimensional torsional mode is suppressed, and panel C when operating in a resonant mode.

3.2. Self-propelled swimming

The conditions considered so far have been primarily positive net thrust conditions. These occur naturally when a propulsor is accelerating, or when a propulsor is attached to a drag-producing body, such that the propulsor must produce net thrust to swim at a constant speed. We are also interested in conditions where the net thrust is zero. In this case, the thrust of the propulsor is equal to its drag, and we say the propulsor is 'self-propelled' or 'free swimming'. These conditions are more relevant for fishes whose propulsive surfaces make up a large portion of the body. The propulsive pectoral fins of rays and skates, for example, account for most of the streamwise-projected body area. When considering the self-propelled swimming speed (u_{SPS}), a propulsive efficiency based on net streamwise forces is zero and thus no longer a useful metric. Instead, we introduce the swimming economy, $\Omega \equiv u_{\mathrm{SPS}}/\bar{P}$, which gives the distance travelled per energy input to the fluid.

Figure 5 shows u_{SPS} and Ω for the three panels at one sample frequency ($f = 2$ Hz) and multiple ground proximities. All three panels show a monotonic increase in self-propelled swimming speed as they approach the ground. The increase is

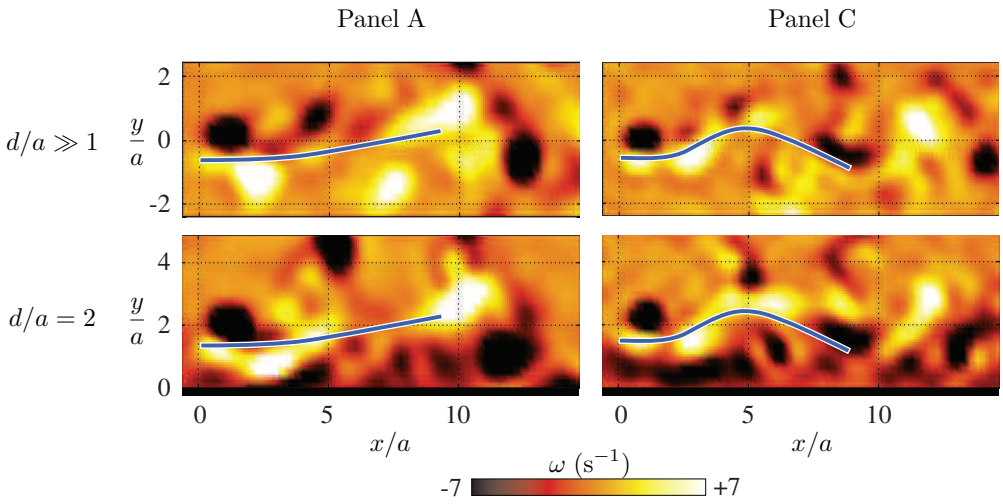

Figure 6. Flow field vorticity (ω) far from and near the ground. Data are taken when the leading edge is closest to the ground ($\phi = \pi$). Flow is left to right, and the black bar indicates the position of the wall in the $d/a = 2$ case.

the most pronounced for panel A, which at $d/a = 2$ swims approximately 25% faster than it does far from the ground. This result is consistent with the net thrust profiles of figure 3, where panel A shows a large increase in thrust at $f = 2$ Hz while the other panels do not. Unlike u_{SPS}, the swimming economy shows no appreciable dependence on ground proximity, that is, the panels maintained a constant cost of transport as they approached the ground.

3.3. Flow field

Figure 6 shows vorticity plots of the surrounding flow field at a sample phase of the cycle during self-propelled swimming. We see that the vorticity is concentrated in boundary layers along the panel and ground, and in vortices caused by separation at the leading and trailing edge. Two leading edge vortices remain attached throughout the cycle. Smaller vortices detach from these primary ones during the cycle, sending negative detached vortices along the top of the panel and positive ones along the bottom. This behavior is seen most clearly for panel A when $d/a \gg 1$. The vortices shed from the trailing edge form the classical reverse von Kármán street of alternating vortices signifying thrust production [26]. Far from the ground these alternating vortices are evenly spaced, while at $d/a = 2$ each negative vortex lags behind and pairs with the next positive vortex shed by the trailing edge. One consequence of this process is an elongation of the positive vortex in the wake resulting from the induced velocity of the nearby negative vortex. This elongation is most clearly visible for panel C when $d/a = 2$.

The ground also introduces lateral asymmetries farther upstream. For example, when $d/a = 2$ the ground distorts the leading edge vortices on the underside of the panels. Consider the positive vortices on the underside of panel A when $d/a \gg 1$. Near the ground, the positive vortex just upstream of the trailing edge is no longer visible. Presumably it has been thoroughly mixed with negative vorticity from the ground boundary layer. The vortex near the leading edge is still visible but has been laterally compressed. In addition, it has rolled up negative boundary layer vorticity into a secondary vortex just downstream.

Unlike the surrounding flow, the kinematics of the panel itself are mostly unaffected by ground proximity. The exception is panel B at frequencies between 1.4 and 1.9 Hz, where the torsional mode is affected by the presence of the ground. For all other cases, any changes observed in the panel kinematics were within the bounds of experimental error. It appears that over the range of conditions considered, the first order effect of the ground is to affect the hydrodynamic forces, but leave the kinematics of the body motion unchanged.

4. Discussion

4.1. Hydrodynamical implications

The lateral and streamwise forces experienced two peaks during the flapping cycle, and these peaks were augmented when operating closer to the ground. The similarity in the behavior of the lateral and streamwise force peaks is to be expected since thrust is the streamwise component of the lift on the panel. The hydrodynamic forces can be separated into circulatory forces (those resulting from the instantaneous pressure field), and added mass forces (those depending on time derivatives of pressure, as governed by the unsteady form of the Bernoulli equation). In general, circulatory forces scale with typical velocities in the flow, while added mass forces scale with typical accelerations in the flow [27]. In the current experiment, the highest near-ground force amplification occurred when the leading edge had high velocity ($\dot{y}_{\mathrm{LE}}$) but low acceleration ($\ddot{y}_{\mathrm{LE}}$). This result suggests that the effects of the ground are more pronounced on circulatory forces than on added mass forces. This observation is consistent with the results in steady ground effect, and it appears generally true that thrust is amplified by ground effect primarily through enhanced circulation. The fact that thrust amplification was in some cases higher on the downstroke than the upstroke is likely due to asymmetries in the surrounding

flow. This effect was also observed in the artificial beetle wings examined by Truong *et al* [19].

When considering time-averaged thrust, the advantages of ground effect were shown to be restricted to certain frequency regimes. This effect contrasts with the results for rigid foils, where thrust amplification is observed at nearly all conditions [18]. The effect may also help to explain the lack of significant benefits observed by Blevins and Lauder (2013) [20], since large portions of the parameter space show no thrust benefits at all. In some regimes where benefits occurred, namely, panels A and B flapping at high frequencies, the thrust nearly doubled near the ground but the propulsive efficiency remained constant. This observation is consistent with the results for rigid airfoils [18], where comparable thrust amplification was observed and propulsive efficiency was found to be independent of ground proximity. In regimes of trailing edge resonance and three-dimensional mode suppression, however, the propulsive efficiency did increase. Thus, for the simple geometry examined here the enhanced efficiency of near-ground propulsion relies on the propulsor being flexible.

All of the panels considered could self-propel faster near the ground, with negligible changes in their costs of transport. That is, for the same energy input, the panels could travel the same distance but in shorter times. Note also that panel A experienced the highest increase in swimming speed, but its absolute swimming economy was the lowest. As mentioned above, panel A also had constant propulsive efficiencies, unlike panels B and C whose efficiencies increased near the ground. Thus, panel A experienced the highest boost in thrust near the ground, but at the cost of no increases in propulsive efficiency and low absolute swimming economies. These results demonstrate the trade-offs between near-ground benefits, efficiency, and economy as the flexibility is varied.

Many of the asymmetric flow features observed near the wall were also observed for rigid propulsors. Wake vortex pairing and wake vortex elongation, for example, were also observed behind pitching rigid airfoils in ground effect [18]. In the rigid case, it was shown numerically that vortex pairing led to nonzero time-averaged lateral forces. No such nonzero forces were observed here; that is, the lateral forces time-averaged to zero in all cases within the experimental resolution. This result helps to explain the constancy of the panel kinematics as the panels approached the ground, an effect also observed for three-dimensional stingray-inspired propulsors [20]. The lack of time-averaged lateral forces may represent another advantage of flexibility near the ground, in that, unlike rigid pitching airfoils, the flexible propulsors considered here can swim steadily at a given ground proximity without needing to counteract a time-averaged lateral force.

4.2. Biological propulsion near surfaces

Many aquatic animals move near surface boundaries using flexible, flapping propulsors, and yet this aspect of animal propulsion has not been studied extensively (but see [1, 2, 6]) compared to the large body of literature on free-swimming. Boundaries can consist of other individuals moving in a swarm, the water surface, the bottom of streams, lakes or the ocean, or vertical surfaces of structured habitats like coral reefs or kelp forests. In addition, many fish species live on the bottom and routinely experience boundary layer flow dynamics as they feed, swim, and reproduce (see, for example, [7, 8]). The dynamics of animals moving near surfaces is a rich area for study: swimming near boundaries might exhibit very different dynamics than free-swimming, and boundary conditions can alter ambient flows so that flow gradients and turbulent eddies can impinge on moving animals and alter their propulsive efficiency and kinematics. Optimal motions for moving in the freestream may not be optimal for moving near surfaces. Furthermore, a number of fish species such as rays and flatfishes undertake long-distance (many hundreds of kilometers) migrations when swimming near the substrate (see [28] for a recent overview of many aspects of fish migration). Even species like eels which undertake long open ocean migrations, move near substrates for extended distances when they enter freshwater and then travel upstream to mature to adulthood. During such long migrations, energy savings by swimming near surfaces may be significant.

We believe, therefore, that the dynamics of animals moving near boundaries needs to be more comprehensively studied. But conducting controlled experimental analyses where parameters such as frequency and body stiffness can be altered is challenging when working with live animals. In this paper we use a mechanical device to produce flapping motions of flexible panels near a rigid wall. We show that efficiency may be increased when swimming near a wall, and that for the more flexible panels the body dynamics are not substantially altered. This suggests that fishes swimming near a boundary may experience energetic advantages due to hydrodynamic effects that are not reflected in altered body and tail kinematics, and that animals showing no kinematic effects of near-wall swimming may still experience locomotor advantages.

The three flexible panels studied here possess flexural stiffnesses that are similar to the range of stiffnesses measured for fresh fish bodies. Eel bodies possess stiffnesses of 1.8×10^2 N mm^2 [29], and passive body stiffness can vary from approximately 1×10^3 N mm^2 near the head to 1 N mm^2 near the tail [30]. The fin rays that form the primary supports in fish fins possess a flexural stiffness of 1–565 N mm^2 [21, 31] depending where along the fin this is measured: the base of fish fin rays is much stiffer than the distal tip region. These values are comparable to the flexural rigidities of the two more flexible panels studied here (table 1), suggesting that this simple flexible panel model is a suitable experimental system for studying moving fish bodies and fins, and that the range of hydrodynamic and energetic effects determined here may well be applicable to swimming fishes.

Since fish can actively alter stiffness during locomotion by activation of body and fin musculature, a number of features of biological propulsion near surfaces may be more complex than is reflected by passive panel swimming. The issue of how much fish can actively alter flexural stiffness of bodies and fins is as yet unresolved, but such active changes during swimming near surfaces may provide fishes with a means of fine tuning thrust and energetic effects as surface characteristics change during migration.

5. Conclusions

Swimming near the ground was shown to provide hydrodynamic benefits to heaving flexible panels. First, near-ground propulsion resulted in higher thrust peaks during the flapping cycle. These peaks occur just after the mid downstroke and mid upstroke. For panel A at $d/a = 2$, the increase in thrust was more pronounced during the downstroke, a result that is consistent with Truong *et al* [19], who also found unsteady ground effect to be slightly stronger on the downstroke.

These higher thrust peaks translate directly to higher time-averaged thrust. When panels A and B were actuated at high flapping frequencies ($>$1.5 Hz and $>$2.25 Hz, respectively), they produced more time-averaged net thrust while keeping their propulsive efficiency constant. Panels B and C showed two additional regimes of near-ground benefits. When panel C was operating in a chordwise resonant mode, swimming near the ground not only increased its thrust but also increased its propulsive efficiency. Efficiency also increased for panel B, but for a different reason. Panel B exhibited a torsional mode over a range of frequencies ($\approx$1–2 Hz) that acted to reduce its net thrust. This mode was suppressed more easily near the ground, resulting in both increased thrust and increased efficiency near the wall.

The kinematics of the panels, with the exception of the torsional mode of panel B, were unaffected by the presence of the boundary. The surrounding flow field, however, showed significant differences near the ground. Lateral asymmetries resulted from leading edge vortex compression, vortex pairing in the wake, and elongated wake vortices. The increases in thrust near the ground were also shown to increase the self-propelled swimming speed. All panels monotonically increased their self-propelled swimming speed as they approached the ground, by as much as 25% for panel A. The swimming economy, however, remained constant, implying that the panels could swim faster near the ground for the same energy cost.

While the planform considered here was non-biological, the hydrodynamic benefits are likely to apply to more complex geometries, especially those where broad flexible propulsors are involved such as fish bodies and fins. The results of figure 3 showed that net thrust increased only over certain ranges of flapping frequencies, and that these ranges depended on the flexibility of the propulsor. To take advantage of unsteady ground effects, near-ground flexible swimmers would need to keep track of these ranges and adjust their actuation accordingly. By doing so, they could produce more thrust by swimming near the ground, and in some cases do so more efficiently.

Acknowledgments

This work was supported by the Office of Naval Research under MURI grant number N00014-08-1-0642 (Program Director Dr Bob Brizzolara), and the National Science Foundation under grant DBI 1062052 (PI Lisa Fauci) and Grant EFRI-0938043 (PI George Lauder).

References

[1] Webb P W 1993 The effect of solid and porous channel walls on steady swimming of steelhead trout *Oncorhynchus mykiss J. Exp. Biol.* **178** 97–108
[2] Blake R W 1979 The energetics of hovering in the mandarin fish *(Synchropus picturatus) J. Exp. Biol.* **82** 25–33
[3] King H M, Shubin N H, Coates M I and Hale M E 2011 Behavioral evidence for the evolution of walking and bounding before terrestriality in sarcopterygian fishes *Proc. Natl Acad. Sci. USA* **52** 21146–51
[4] Macesic L J and Kajiura S M 2010 Comparative punting kinematics and pelvic fin musculature of benthic batoids *J. Morphol.* **271** 1219–28
[5] Wilga C D and Lauder G V 2001 Functional morphology of the pectoral fins in bamboo sharks, chiloscyllium plagiosum: benthic versus pelagic station-holding *J. Morphol.* **249** 195–209
[6] Webb P W 2002 Kinematics of plaice, pleuronectes platessa, and cod, gadus morhua, swimming near the bottom *J. Exp. Biol.* **205** 2125–34
[7] Coombs S, Anderson E, Braun C B and Grosenbaugh M A 2007 The hydrodynamic footprint of a benthic, sedentary fish in unidirectional flow *J. Acoust. Soc. Am.* **122** 1227–37
[8] Carlson R L and Lauder G V 2010 Living on the bottom: kinematics of benthic station-holding in darter fishes (percidae: Etheostomatinae) *J. Morphol.* **271** 25–35
[9] Rozhdestvensky K V 2006 Wing-in-ground effect vehicles *Prog. Aerospace Sci.* **42** 211–83
[10] Baudinette R V and Schmidt-Nielsen K 1974 Energy cost of gliding flight in herring gulls *Nature* **248** 83–4
[11] Blake R W 1983 Mechanics of gliding birds with special reference to the influence of ground effect *J. Biomech.* **16** 649–54
[12] Hainsworth F R 1988 Induced drag savings from ground effect and formation flight in brown pelicans *J. Exp. Biol.* **135** 431–44
[13] Rayner J M V 1991 On the aerodynamics of animal flight in ground effect *Phil. Trans. Biol. Sci.* **334** 119–28
[14] Nowroozi B N, Strother J A, Horton J M, Summers A P and Brainerd E L 2009 Whole-body lift and ground effect during pectoral fin locomotion in the northern spearnose poacher (agonopsis vulsa) *Zoology* **112** 393–402
[15] Park H and Choi H 2010 Aerodynamic characteristics of flying fish in gliding flight *J. Exp. Biol.* **213** 3269–79
[16] Tanida Y 2001 Ground effect in flight *Japan Soc. Mech. Eng.* **44** 481–6
[17] Iosilevskii G 2008 Asymptotic theory of an oscillating wing section in weak ground effect *Eur. J. Mech.* **27** 477–90
[18] Quinn D B, Moored K W, Dewey P A and Smits A J 2014 Unsteady propulsion near a solid boundary *J. Fluid Mech.* **742** 152–70
[19] Truong T V, Byun D, Kim M J, Yoon K J and Park H C 2013 Aerodynamic forces and flow structures of the leading edge vortex on a flapping wing considering ground effect *Bioinspir. Biomim.* **8** 036007
[20] Blevins E and Lauder G V 2013 Swimming near the substrate: a simple robotic model of stingray locomotion *Bioinspir. Biomim.* **8** 016005
[21] Lauder G V, Lim J, Shelton R, Witt C, Anderson E and Tangorra J L 2011 Robotic models for studying undulatory locomotion in fishes *Mar. Technol. Soc. J.* **45** 41–55
[22] Lauder G V, Flammang B E and Alben S 2012 Passive robotic models of propulsion by the bodies and caudal fins of fish *Int. Comput. Biol.* **52** 576–87

[23] Blevins E and Lauder G V 2012 Rajiform locomotion: three-dimensional kinematics of the pectoral fin surface during swimming by freshwater stingray *Potamotrygon orbignyi* *J. Exp. Biol.* **215** 3231–41
[24] Stanislas M, Okamoto K, Kahler C J and Westerweel J 2005 Main results of the second international PIV challenge *Exp. Fluids* **39** 170–91
[25] Quinn D B, Lauder G V and Smits A J 2014 Scaling the propulsive performance of heaving flexible panels *J. Fluid Mech.* **738** 250–67
[26] Koochesfahani M M 1989 Vortical patterns in the wake of an oscillating airfoil *AIAA J.* **27** 1200–5
[27] Katz J and Plotkin A 2001 *Low-Speed Aerodynamics* 13th edn (Cambridge: Cambridge University Press)
[28] Ueda H and Tsukamoto K 2013 *Physiology and Ecology of Fish Migration* (Boca Raton, FL: CRC Press)
[29] Long J H 1998 Muscles, elastic energy, and the dynamics of body stiffness in swimming eels *Am. Zool.* **38** 771–92
[30] McHenry M J, Pell C A and Long J A 1995 Mechanical control of swimming speed: stiffness and axial wave form in undulating fish models *J. Exp. Biol.* **198** 2293–305
[31] Flammang B E, Alben S, Madden P G A and Lauder G V 2013 Functional morphology of the fin rays of teleost fishes *J. Morphol.* **274** 1044–59